Coupling Between Acoustic Velocity Oscillations and Solid-Propellant Combustion

R. S. Brown,* A. M. Blackner,† P. G. Willoughby,‡ and R. Dunlap§
United Technologies Corporation, San Jose, California

The fluid mechanics of the coupling between acoustic waves and the solid-propellant combustion have been studied in a cold-flow simulation of a solid-propellant rocket motor. The axial variation of the oscillatory heat flux shows substantial deviations from the behavior expected from both the linear and nonlinear heuristic models of velocity coupling that are currently used in combustion stability analyses. At low acoustic pressure (0.05%), the acoustic waves generate oscillatory heat-transfer coefficients at axial positions upstream of the transition in the mean velocity. Yet the nonlinear model suggests no flux oscillations should occur there. Downstream of the mean flow transition however, where both models predict significant flux oscillations will occur, there is no influence of the acoustic waves on the oscillatory heat-transfer coefficient. At higher acoustic pressures (0.5%), nonlinear heat-transfer coefficients are generated upstream of the transition, but not at the mean flow transition as expected from the nonlinear model. Yet, downstream of this transition, the acoustic velocities do produce a linear heat-transfer response. The axial drop in the static pressure and the radial profiles of the total pressure show the mean flow follows the expected rotational inviscid turbulent behavior. Based on these results, the model for velocity coupling in combustion stability analyses requires significant revision. Additionally, linear acoustic behavior is limited to acoustic pressures below 0.1%, which is an order of magnitude below the levels currently used.

Nomenclature

a = experimental coefficient
A = area
b = experimental coefficient
D = diameter
E = volts
f = frequency
h = heat transfer coefficient
M = Mach number
P = pressure
r = radius
R = resistance
t = time
T = temperature
Z = axial position
α = damping time constant
γ = specific heat ratio
ϵ = normalized head-end acoustic pressure ($\hat{P}/\gamma\bar{P}$)
ρ = density

Subscripts

b = surface blowing
g = gage
L = loss
n = nitrogen
w = wall

Superscripts

$\bar{(\ )}$ = mean
$\hat{(\ )}$ = complex amplitude

Received Nov. 1985; revision received April 14, 1986.

*Senior Staff Scientist, Chemical Systems Division. Associate Fellow AIAA.
†Research Engineer, Chemical Systems Division.
‡Senior Staff Scientist, Chemical Systems Division.
§Senior Staff Scientist, Chemical Systems Division. Member AIAA.

Introduction

COUPLING between velocity oscillations and the combustion zone of solid propellants has been recognized for many years as a potential contributor to the overall acoustic energy balance in the evaluation of the combustion stability. Hart et al.[1] and Price[2] discussed this coupling in their early combustion stability studies. Later, Price[3] proposed a nonlinear heuristic model for this coupling to explain qualitatively the acoustic energy gains and losses, nonlinear wave forms, and burning rate changes observed in unstable motors. In this model, oscillatory heat transfer to the burning propellant surface was assumed to be the dominant mechanism coupling the acoustic velocity to the combustion. By analogy to erosive burning, a threshold velocity was assumed to characterize the velocity coupling, although the two threshold velocities were not required to be identical. This hypothesis led to a qualitative framework explaining mean flow effects on the velocity-coupled response function, rectification effects that would produce nonlinear wave forms, and flow reversal effects that would also generate nonlinear wave forms when the acoustic velocity exceeds the local mean speed. Subsequently, Dehority and Price[4] studied the properties of this framework parametrically. Although it has been used successfully to correct a number of motor instabilities, this framework still lacks verification of the mechanistic foundation needed for quantitative motor design purposes.

Culick[5] subsequently proposed a simple linear velocity response function model based on the solid-phase thermal lag model for the pressure-coupled response function. This linear model would apply in Price's framework when the total velocity (mean plus oscillatory velocity) exceeds the threshold, yet subsequent applications of this linear model have ignored this restriction. Lengelle[6] used a turbulent boundary-layer analysis to predict the oscillatory heat-transfer flux to the propellant surface and developed an expression that is functionally identical to Culick's expression. Micheli[7] also proposed slight modifications to Culick's model and Condon[8] attempted to add particle size effects to the response model.

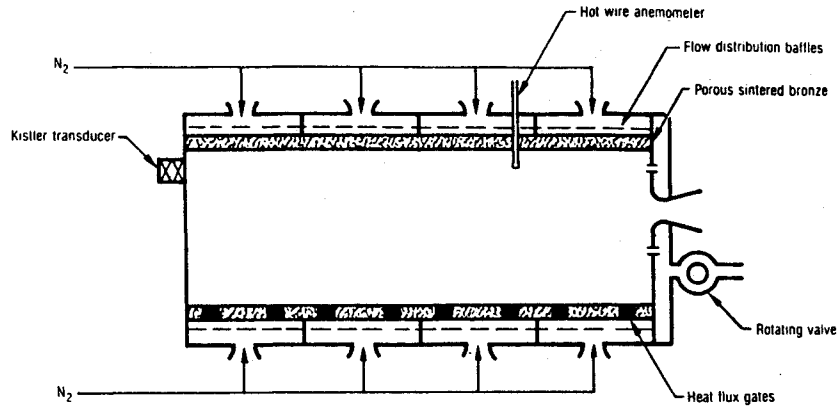

Fig. 1 Cold-flow velocity coupling apparatus.

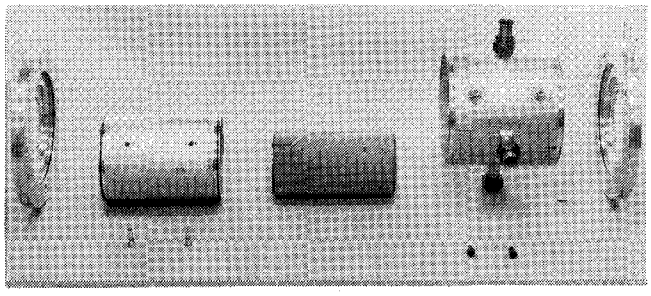

Fig. 2 Exploded view of a "segment."

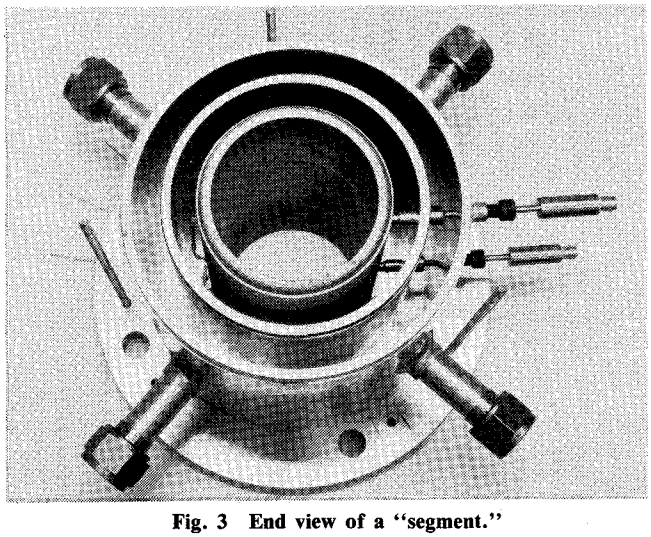

Fig. 3 End view of a "segment."

Measured linear velocity-coupled response functions were first reported by Stepp[9] using a modified T-burner. Improvements in the T-burner were made by Beckstead[10] and Micheli[7] to permit testing with aluminized propellants. More recently, Brown[11] explored the dual rotating valve approach, while Micci et al.[12] examined the modulated throat motor for making these response measurements. All of these studies reported numbers for the linear velocity-coupled response function that were derived from acoustic models of the particular experiment. The measured magnitude and phase (with respect to the acoustic driving) of these derived response functions differ significantly from the expected values. This difference suggests significant errors in either the experiments or the models used to interpret the data. These experimental studies, together with the earlier tests of Crump and Price[13] and Nadaud and Gigguel[14] did, however, provide secondary evidence suggesting that some form of nonlinear velocity behavior does occur because nonlinear pressure oscillations have been observed under conditions thought to have high-velocity coupling.

Velocity coupling effects have also been incorporated in motor stability predictions.[15] However, Glick and Kirschner[16] and Brown et al.[17] have noted large discrepancies between the stability predictions and subsequent motor experience where the velocity coupling effects were predicted to be large. Thus, motor experience also suggests there are serious deficiencies in the velocity coupling models.

Recently, Price[18] discussed a number of inconsistencies in the interpretation of velocity coupling, as well as the limitations in the understanding of the basic mechanism involved. For example, he noted that motor stability predictions treat the velocity response as a propellant property that is independent of position in the motor. This requires the response be independent of the mean flow environment. Yet the dominant mechanism is assumed to be oscillatory heat transfer from the gas phase into the solid phase, which depends on both the mean flow and acoustic environment. Hence, the assumption that the oscillatory heat transfer is flow related and simultaneously independent of position in the motor is inconsistent. In addition, most investigators assume that turbulent boundary-layer behavior characterizes the flow; yet Culick,[19] Beddini,[20] and Dunlap et al.[21] have found the mean flow to be rotational and inviscid and not at all characterized by a turbulent boundary layer.

Russian investigators have also analyzed velocity coupling on the basis of turbulent boundary-layer behavior. Gotintsev and Pokhil[22] and Medvedev and Revyagin[23] both report measuring a threshold mean flow velocity for velocity coupling. They also note that this threshold velocity is approximately half the one for erosive burning. Precisely how these measurements were made and the acoustic pressure levels observed were not reported. Neither investigator compared their results with the models described above.

Discussions at the JANNAF Workshop on Velocity Coupling[24] focused on yet another difficulty in the turbulent boundary-layer model of velocity coupling. The concensus was that current information, especially from laboratory burners, suggests that the threshold for velocity coupling differs significantly from the threshold velocity for erosive burning. In fact, some investigators felt that there may not be a threshold for velocity coupling at all. This hypothesis suggests that the thickness of the acoustic boundary layer is substantially different from the thickness of the mean flow boundary layer, thereby contradicting the assumption of a quasisteady gas phase. Flandro,[25,26] Hedge et al.,[27] and BenReuven[28] relaxed the quasisteady gas-phase assumption in their analytic studies to include acoustic boundary-layer effects. Their predictions suggested that significant gas-phase lags can be generated for velocity oscillations both normal and parallel to the surface.

This review indicates that there are major limitations in the current understanding of the velocity coupling process.

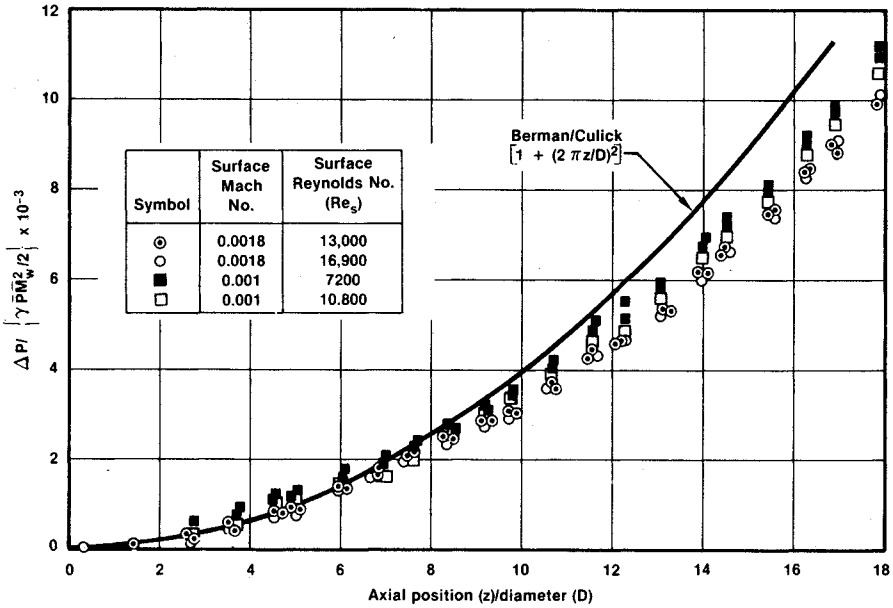

Fig. 4 Axial pressure drop results.

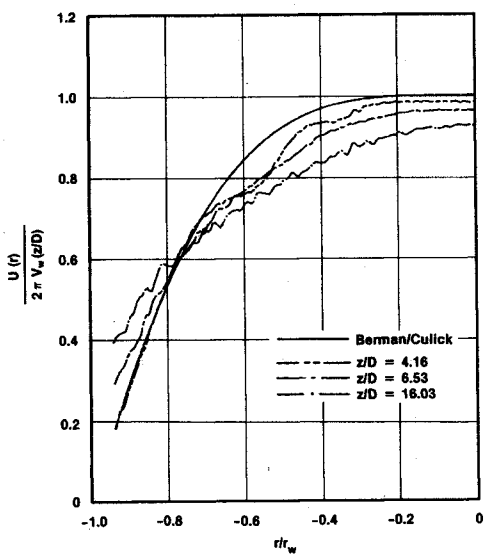

Fig. 5 Velocity profiles from total pressure.

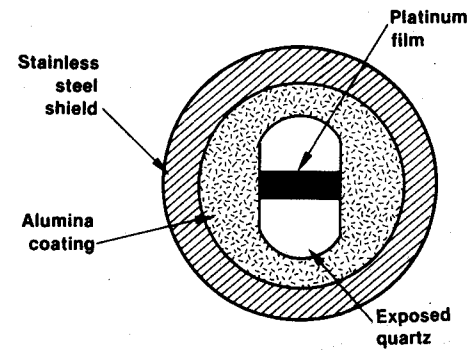

Fig. 6 Hot-film gage construction.

In particular, it is apparent that the basic mechanisms and basic characteristics of this coupling have not been defined. Hence, there is little insight into this coupling mechanism and how it influences the overall combustion stability under rocket flow conditions. In addition, a number of inconsistencies have been noted in the current qualitative treatment of velocity coupling. Obviously, a basic study of this coupling is needed to clarify the major issues noted above. This paper presents experimental results that address one of these issues, namely, the effect of velocity oscillations on the oscillatory heat transfer to the surface with a relatively high blowing rate. An experimental approach was selected because of the unique character of the internal flowfield in a solid-propellant rocket and the need for data against which to compare mechanistic concepts.

Experimental Apparatus

To conduct the experiments, the cold-flow apparatus shown schematically in Fig. 1 was constructed. Nitrogen flowing through porous cylindrical bronze tubes simulated the gas evolution by the propellant combustion and generated a realistic internal flowfield. In previous studies,[21,29,30] this technique has been used successfully to investigate the steady-state and oscillatory properties of the flow. Considerable care was taken to ensure that the surface Mach number was constant over the entire simulated burning surface. A flow distribution tube was used to equalize the flow circumferentially around the 10 cm diam porous tube.

The apparatus was constructed in eight sections that join together to form a continuous surface. The nitrogen flow into each of these sections was sonically choked to further equalize the flow. Figure 2 shows an exploded view of one section, while an end view is shown in Fig. 3. Each section has two ports for heat flux gages (shown installed in Fig. 3) or for hot-wire anemometers. Pressure taps were also located on the simulated propellant surface at three axial stations, with one tap between the porous tube and the flow distribution tube at each section. Leads from these taps were attached to a Scanivalve/pressure transducer multiplexing system for recording the mean pressures throughout the apparatus. Kistler pressure transducers were mounted at both ends of the apparatus. The heat flux gages were connected to TSI model 1050 anemometers that were operated in the constant-temperature mode. Hence, the power to the gage measured the heat transfer directly, with a frequency response of 10 kHz.

Flow oscillations were generated by a rotating valve at the aft end. A specially designed aft section was fabricated to mount a fixed-diameter sonic exhaust nozzle on the centerline and to minimize the radial distortion of the velocity oscillations entering the port from the rotating valve. A variable-speed drive electric motor connected to the rotating

valve controlled the frequency of the acoustic oscillations. The hole/slot geometry in the rotating valve produced nearly pure sine wave oscillations: 91% at the driving frequency, 4.5% at the third harmonic, and 4.5% at the higher odd harmonics.[31]

Exploratory Steady Flowfield Measurements

The initial experimental studies were directed toward defining the general characteristics of the mean flowfield. Towards the head end, Beddini[20] predicted that the flow follows the rotational inviscid behavior first analyzed by Taylor[32] and Culick.[19] This behavior was subsequently verified experimentally by Dunlap et al.[21] and Yogodkin[33] in cold-flow tests using hot-wire anemometers. (Beddini's thesis also contains an excellent review of both the experimental and analytical state of knowledge of the mean flow.) Beddini also predicted that at some critical length-to-diameter ratio, which he estimated to be between 4 and 10, the flow would transition toward turbulent flow in a pipe. Hence, the initial studies were conducted to explore the validity of Beddini's transition predictions.

Tests were first conducted to compare measured axial pressure drops with predictions based on the Taylor/Culick model. This model yields the equation

$$\frac{2\Delta P}{\gamma \bar{P}(r_w,Z)M_w} = 1 + \left(\frac{2\pi Z}{D}\right)^2 \qquad (1)$$

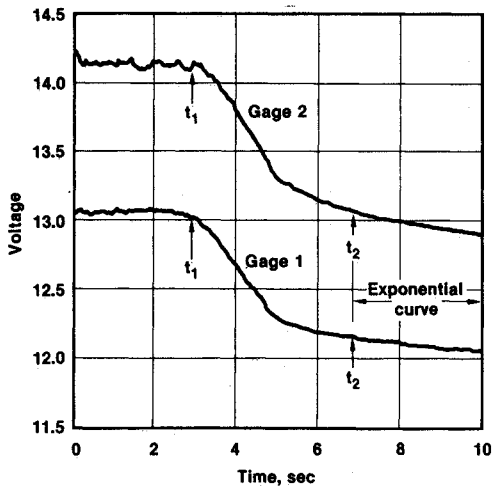

Fig. 7 Voltages from heat flux gages.

The measurements were made by connecting one side of a high-sensitivity ΔP transducer to the head end of the apparatus on the centerline (i.e., $r=0$). The other side of the transducer was connected through a Scanivalve to the pressure taps on the surface of the simulated propellant. This provided three pressure measurements for each of the eight sections used in these tests. In effect, the Scanivalve multiplexes the pressure taps to the pressure transducer. By stepping the Scanivalve every 0.8 s, the axial static pressure profile could be measured in 35 s.

Figure 4 compares the measured pressure drop data with Eq. (1) for two surface Mach numbers and two surface Reynolds numbers at each Mach number. The data agree with the predicted pressure drop profile for Z/D less than 7 to 8. This agreement indicates that flow is rational and inviscid for Z/D less than 7 to 8. Furthermore, the surface Reynolds number effect is very small, indicating, as Dunlap noted, that viscous forces are small in this region. For greater values of Z/D, the measured pressure drops begin to diverge from the Taylor/Culick model. This deviation is in a direction suggesting the velocity profile becomes flatter in the core flow region, which is consistent with Beddini's flow field prediction.[20] Moreover, the transition actually begins at the axial location very close to the location predicted by Beddini.

Mean velocity profiles were measured using a Keil probe to detect the total pressure. This probe was traversed slowly and continuously across the port diameter using a linear traverse manufactured by the L. C. Smith Co. To determine the radial profile of the dynamic pressure, one leg of a high-sensitivity differential pressure transducer was connected to the static pressure tap just downstream of the probe location and the other leg to the Keil probe. The static pressure drop data shown in Fig. 4 were used to correct the measurements for the small drop in pressure between the probe and static pressure tap.

Figure 5 shows the velocity profiles derived from the total pressure profile at three axial stations: at $Z/D=4.16$ where the axial pressure drop agrees with the rotational inviscid flow model, at $Z/D=6.53$ where the first deviations from the rotational inviscid flow occur, and at $Z/D=16$ where the deviation from the model is substantial. For comparison, the predicted axial velocity profile is also shown. These experimental results show good qualitative agreement with the behavior predicted by Beddini. It should be noted that the dead-band errors in positioning the traverse and the continuous motion of the probe make more detailed quantitative comparisons inappropriate. Those quantitative comparisons are currently the subject of a detailed study.[34]

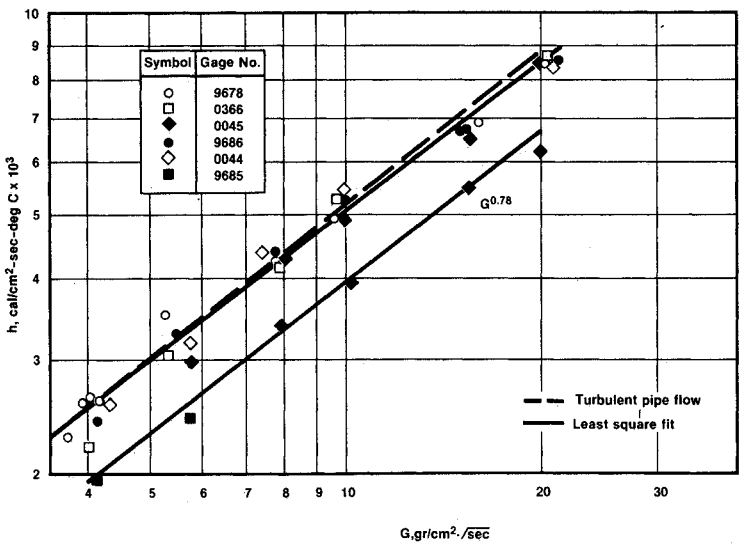

Fig. 8 Heat-transfer gage calibration in 4 in. pipe.

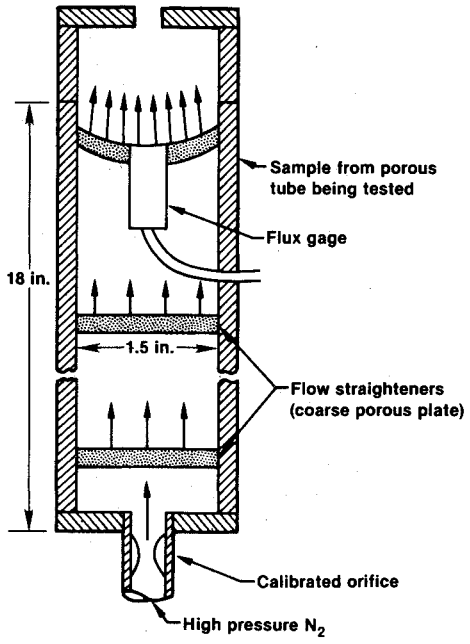

Fig. 9 Apparatus to calibrate heat loss.

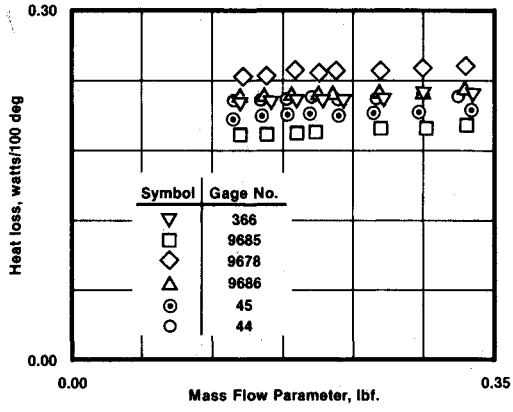

Fig. 10 Heat loss calibration data.

Characteristics of Heat Flux Gages

The primary objective of these studies was to measure the oscillatory heat flux at the simulated propellant surface. Therefore, the characteristics of the heat-transfer gages were explored in some detail. Figure 6 shows the construction of these gages (model 1237 manufactured by TSI, Inc.). In this application, the gages (specifically the platinum film on the end of each gage) were operated in the constant-temperature mode (i.e., constant gage resistance). When operated in this mode, a feedback circuit in the anemometer signal conditioner maintains a constant film temperature fluctuation up to 10 kHz. The instantaneous energy balance for the gage is given by

$$h(t)A_g(T_g - T_n) = \frac{R_g[E^2(t) - E_L^2(t)]}{(R_g + 41.1)^2} \qquad (2)$$

loss to gas = electrical input − side wall losses

Three questions arose in using this energy balance. What is the magnitude and time dependence of the energy loss term? What is the effective area of the gage for heat transfer to the gas (i.e., is it the area of the platinum film, the exposed quartz)? Are the relatively large side-wall losses independent of the flow oscillations through the porous tubing?

Exploratory tests indicated that the steady-state gage voltage was typically of the order of 14 V under cold-flow conditions and approximately 11 V under nonflowing conditions. This behavior indicates that the side-wall heat losses were substantial and therefore needed to be characterized. Thermal analyses of the gage were then conducted to estimate the temperature profiles in the quartz substrate. Two side-wall boundary conditions were considered. The first assumed a high thermal resistance to be present between the outer gage wall and the surrounding material, such as transfer through a gas film to the porous bronze or transfer to a plastic material. With this boundary condition, the temperature was predicted to be essentially constant across the circular end face of the gage. This suggests that, under these conditions, the exposed oval section on the end surface is the thermally active area of the gage.

The second side-wall boundary condition assumed that the side-wall temperature equaled the temperature of the material surrounding the gage. This second condition models the situation wherein the thermal conductivity of the porous bronze dominates the gage losses. With this condition, the surface temperature on the end face drops rapidly with increasing distance from the constant-temperature platinum film. This finding suggests the area of the platinum film is thermally active under high-loss conditions.

Two series of tests were then conducted to validate these analytical predictions. In the first series, the gages were exposed to a fully developed turbulent pipe flow of nitrogen. Specificially, the gages were mounted in a plastic block attached to the wall of a 10 cm diam 7 m long plastic pipe having a smooth internal wall. The end surface of the gage was flush with the inner surface of the pipe. Nitrogen entered the pipe through a sonic choke into one end of the pipe and exhausted through a second choke at the other end. The gage was located approximately 0.6 m upstream of the exhaust choke.

Figure 7 shows a typical voltage-time record. At t_1, the nitrogen flow was turned off and the pipe allowed to blow down to ambient pressure at t_2. For times greater than t_2, the gage heated the surrounding mounting block that had been cooled by the expanding nitrogen. Hence, the heat losses from the gage decreased with time, accounting for the continually decreasing gage voltage with time. This heating follows the equation,

$$\ell n[E_L(t)] = at + b \qquad (3)$$

Equation (3) was then used to extrapolate E_L to t_1, thereby providing an estimate for the voltage characterizing the heat losses under steady flow conditions.

Using this procedure for characterizing the heat losses, measured heat-transfer coefficients (based on the area of the exposed quartz) were derived and compared in Fig. 8 to the standard correlation of turbulent pipe flow data. Note that excellent agreement was obtained with five of the gages, whereas the sixth gage was 30% lower. (The source of this discrepancy could not be determined.) This agreement for the five gages supports the analytical predictions that suggested the entire exposed end area is thermally active when the sidewall losses are characterized by a high thermal resistance.

The second series of tests was conducted to evaluate the gage behavior under high heat loss conditions. Specificially, the gages were mounted in a sample of the porous bronze using the same methods employed in the cylindrical port apparatus. Figure 9 shows the test configuration for these high heat loss tests. This apparatus minimized the effect of gas flow across the end face of the gage. Tests were conducted at two surface Mach numbers (0.001 and 0.0018) over a range of nitrogen mass flow rates.

Figure 10 shows the measured heat losses [determined by setting $h(t) = 0$ in Eq. (2)] as a function of nitrogen mass

flow (as determined by the pressure upstream of the exhaust choke and the choke diameter). These data show the heat losses to be independent of the gas flow through the porous bronze, which indicates that the temperature of the porous bronze and the nitrogen are equal and that conduction from the gage to the bronze controls the heat loss. This behavior might have been expected because the surface area for conduction from the gage to the bronze is much smaller than the area for transferring energy from the bronze to the nitrogen.

Several conclusions can be drawn from these gage characterization studies. First, the area of the platinum film approximates the thermally active end area of the gage in the porous wall experiment. Second, gas flow oscillations through the bronze that result from the finite admittance of the bronze, do not produce oscillatory sidewall losses from the gage. Finally, the active gage areas are small and, therefore, negligible energy is transferred to the nitrogen. Thus, in Eq. (2), T_g, T_n, and E_L are independent of time. In addition, the oscillatory voltages are typically small, so the oscillating heat-transfer coefficient generated by the acoustic waves can be derived from the oscillating voltage measurements by linearizing Eq. (2) to

$$\hat{h}A\ (\bar{T}_g - \bar{T}_n) = \frac{2\hat{E}\bar{E}R_g}{(R_g + 41.1)^2} \tag{4}$$

Oscillatory Heat-Transfer Measurements

The next series of tests was conducted to measure the oscillatory heat-transfer coefficients as a function of axial position under various flow conditions. Oscillations were driven at approximately 85 and 170 Hz, corresponding to the first two axial acoustic modes of the chamber. Two rotating valves, having different orifice sizes, were used to vary the acoustic pressure level. Signals from all six flux gages, as well as the signals from the head end and two aft-end kistler pressure transducers and the optical tachometer, were recorded of FM tape for later spectral analysis. The optical tachometer signal was particularly useful as a trigger signal for coherently averaging the spectra with the driver of the oscillations. By reversing the head end closure and aft end nozzle and rotating valve fixture, heat-transfer coefficients from 12 axial stations were obtained.

Table 1 Summary of acoustic pressures measurements

Surface Mach no. $\times 10^3$	Driving area	Driving frequency, Hz	Acoustic pressure $\hat{P}/\gamma\bar{P}$,% Head end	Aft end
1.73	0.6%	76	0.055	0.075
		170	0.049	0.092
0.95	1.1%	85	0.061	0.078
		170	0.048	0.087
1.81	3.3%	85	0.39	0.57
		170	0.35	0.73
1.03	5.9%	85	0.43	0.55
		165	0.38	0.73

Two forms of spectral analysis were conducted because the heat flux oscillations included the response to the driven oscillations, as well as the response to any turbulence in the flow. In the first form of analysis, the heat-transfer coefficient spectra were derived from power spectra and, thus, include both the response to the driven oscillations and flow turbulence. In the second form, the oscillatory heat-transfer coefficient spectra were derived from 50 ensembles of the linear spectra that were coherently averaged using the optical tachometer signal as a trigger source. This second form removed much of the turbulence effect, leaving only the response to the driven oscillations.

In both forms of analysis, Eq. (2) could have been used to normalize the oscillatory heat-transfer coefficients to the corresponding mean values. However, when the flux gages were mounted in the porous bronze, the heat losses were much higher than when the gages were mounted in the plastic pipe. Thus, E and E_L have very similar magnitudes. Therefore, the mean heat-transfer coefficient is determined by the small difference in two large numbers and is very sensitive to small errors in either voltage measurement. These voltage errors could have masked the behavior of the normalized coefficients. To eliminate this problem, the un-normalized coefficients are reported.

Figures 11-18 present the heat-transfer coefficient spectra as a function of axial position for eight test conditions: two driving frequencies, two acoustic pressure amplitudes, and two surface Mach numbers. Each figure shows two waterfall plots, one from the power spectral analysis (a) and the other from the coherently averaged spectra (b). The head- and aft-end acoustic pressures that were measured at these same test conditions are presented in Table 1.

A number of important observations can be derived from these results. First, the power spectral plots show a substan-

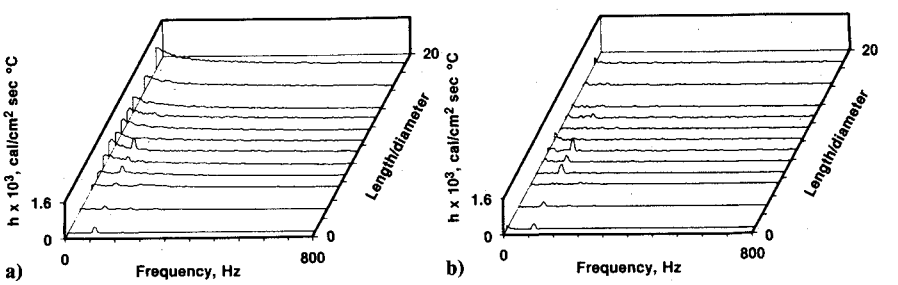

Fig. 11 Oscillatory heat-transfer coefficient spectra ($\bar{\varepsilon} = 0.61\%$, $f = 84$ Hz, $\bar{M}_w = 0.001$).

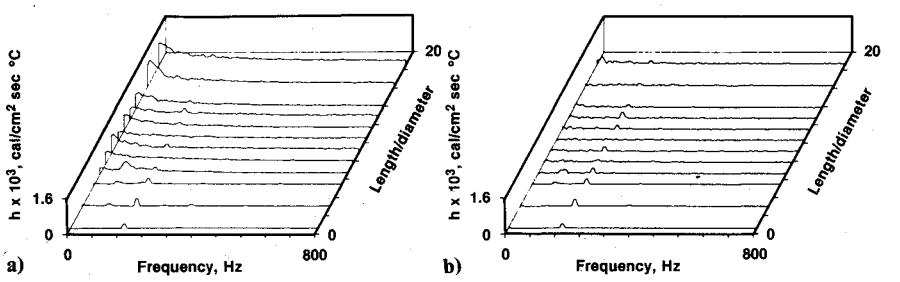

Fig. 12 Oscillatory heat-transfer coefficient spectra ($\bar{\varepsilon} = 0.048\%$, $f = 176$ Hz, $M_w = 0.00095$).

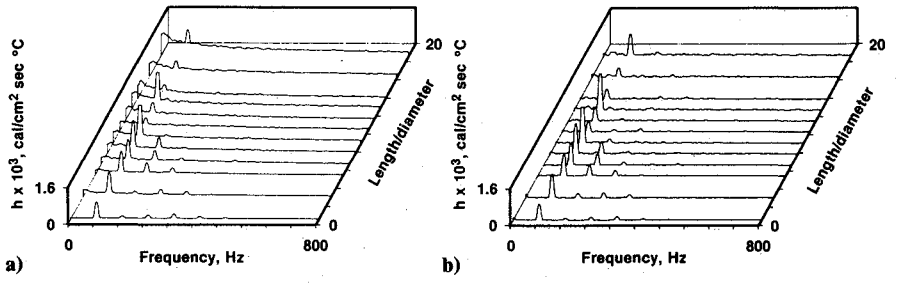

Fig. 13 Oscillatory heat-transfer coefficient spectra ($\varepsilon = 0.43\%$, $f = 85$ Hz, $M_w = 0.00095$).

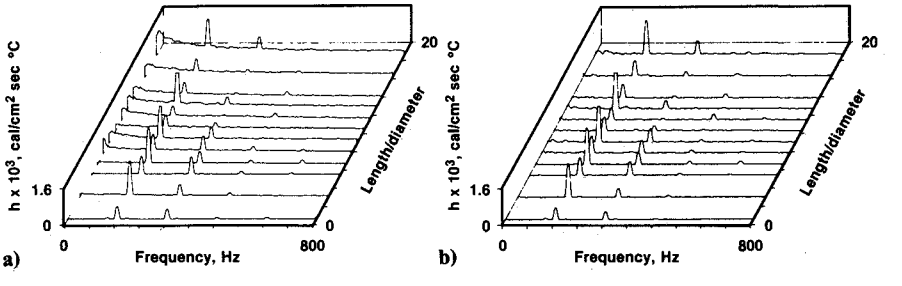

Fig. 14 Oscillatory heat-transfer coefficient spectra ($\varepsilon = 0.38\%$, $f = 165$ Hz, $M_w = 0.001$).

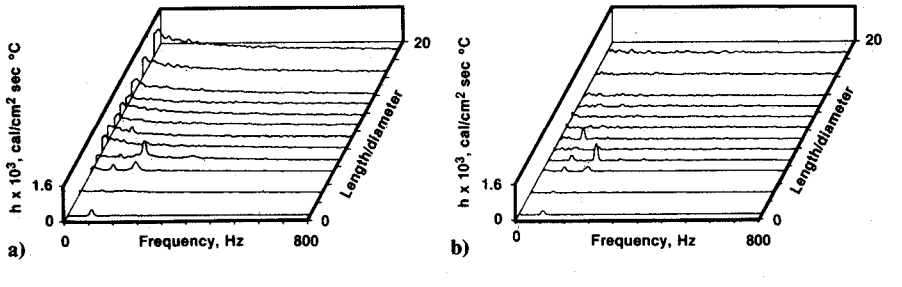

Fig. 15 Oscillatory heat-transfer coefficient spectra ($\varepsilon = 0.055\%$, $f = 78$ Hz, $M_w = 0.0017$).

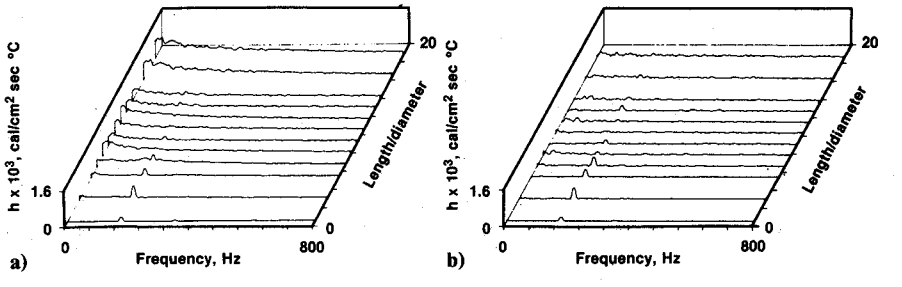

Fig. 16 Oscillatory heat-transfer coefficient spectra ($\varepsilon = 0.49\%$, $f = 175$ Hz, $M_w = 0.0017$).

tial increase in the noncoherent (i.e., turbulent background) fluctuations at axial locations greater than 7 diam from the head end. This indicates that turbulence in the gas flow has penetrated to the wall. Note also that the axial pressure drop data deviate from the rotational inviscid profiles downstream of these same locations. Thus, both the heat-transfer coefficient and pressure drop results are consistent with the flow transition predictions by Beddini.[20]

A second observation results from examining the axial variation of the heat-transfer spectra. For all test conditions, heat-transfer coefficient oscillations were generated by the acoustic oscillations upstream of the mean flow transition, even at the lowest acoustic pressure amplitudes (i.e., 0.05%). Downstream of the flow transition, there were no coherent heat-transfer coefficient oscillations at the lower acoustic pressure amplitudes. However, at the higher pressure amplitudes, the heat-transfer coefficient oscillations are observed at all axial locations.

This behavior was also demonstrated by the axial variation of the coherence between the head-end acoustic pressure and the heat-transfer oscillation shown in Fig. 19. At the low driving amplitude, high coherence was observed only at the head end. As the amplitude of the driving was increased, the region of high coherence spread downstream and eventually covered the entire length of the chamber.

These results are completely inconsistent with the behavior expected from both the linear and nonlinear velocity coupling models. According to the linear model, the oscillatory heat-transfer coefficient should vary sinusiodally with axial position in response to acoustic waves at the lower (fundamental) frequency. At the higher (first harmonic) frequency, the axial variation of the heat-transfer coefficient should be a maximum at Z/L of 0.25 and 0.75, which correspond to the location of the acoustic velocity maxima. Neither pattern was observed.

According to the nonlinear model, the oscillatory heat-transfer coefficient should not respond to the acoustic waves until some threshold velocity is exceeded. Downstream of the threshold, the linear model should apply. Hence, no heat-transfer response would be expected near the head of the chamber, but a response would be expected towards the aft end. In addition, nonlinear behavior would be expected when the sum of the acoustic and mean velocities equals the threshold velocity. Presumably, this condition would occur

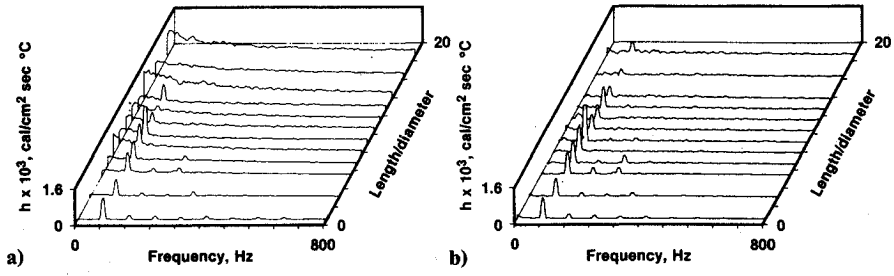

Fig. 17 Oscillatory heat-transfer coefficient spectra ($\varepsilon = 0.39\%$, $f = 85$ Hz, $M_w = 0.0018$).

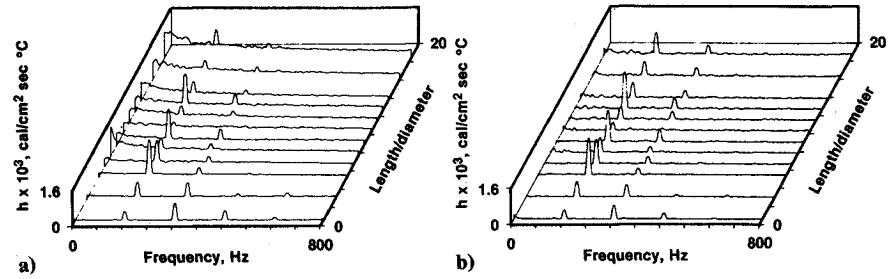

Fig. 18 Oscillatory heat-transfer coefficient spectra ($\varepsilon = 0.35\%$, $f = 170$ Hz, $M_w = 0.0018$).

at some intermediate axial location. Clearly, none of these characteristics are observed in the data. Thus, the validity of both models is highly suspect, which may explain why stability predictions have been very misleading when velocity coupling contributions were predicted to be large.

A third observation is that significant harmonic content is generated at the higher frequencies and at the higher acoustic pressures (0.4%). Initially, the harmonics appear upstream of the mean flow transition and, in fact, are most apparent near the head of the chamber. Interestingly, these harmonics are also observed in the corresponding acoustic pressures.

The higher acoustic pressures were generated using one rotating valve, while the lower amplitudes were generated with a different smaller valve. Hence, the wave form of the area oscillation in the larger valve might have been responsible for the harmonic content. To check its characteristics, the larger valve was connected to a short length, large-diameter chamber operated in the low-frequency bulk mode. The nitrogen flow into and out of this chamber was sonically choked. Spectral analyses of the acoustic pressures showed that no oscillatory energy was generated at harmonic frequencies of the driving frequency. In addition, the coherence between the highly nonlinear optical tachometer signal and the pressure oscillations was very low (i.e., <0.1) at the harmonic frequencies, but was high (0.99) at the driving frequency. These results are consistent with Brown's observation[31] that the hole/slot geometry produces waves having a very low harmonic content. Therefore, the nonlinear behavior observed in the heat-transfer coefficient results from the flow and acoustic environment and not from the acoustic driver.

The generation of harmonic frequency components in the heat-transfer coefficient at high acoustic pressures (i.e., 0.4%) has significant impact on many aspects of the combustion stability problem. It has generally been assumed that linear behavior is valid when the acoustic pressure is below 1%. However, these tests demonstrate that linear behavior is limited to acoustic pressures below 0.1%. Thus, a careful re-examination of all laboratory burner and small-motor results must be made to determine the validity of conclusions derived from linear interpretations.

Approximate Analysis of Oscillatory Heat Flux

A very simplified analysis of the oscillatory heat transfer was conducted to gain some further insights into these data. The primary intent was to determine if the oscillatory heat-transfer coefficient is consistent with the convective heat

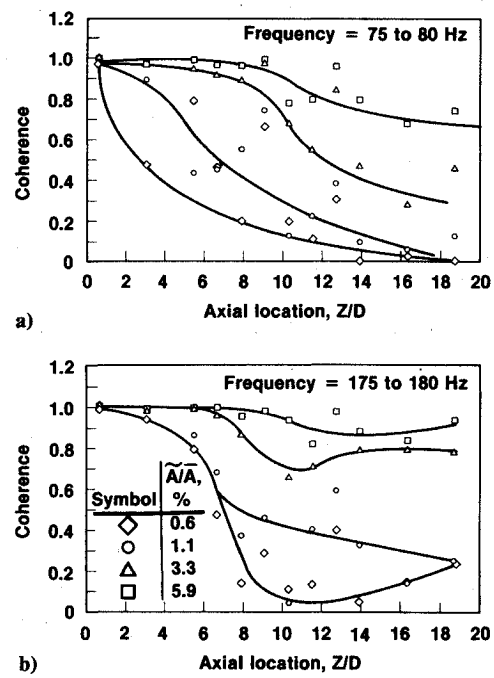

Fig. 19 Coherence between heat transfer and head-end acoustic pressure: a) Frequency = 75-80 Hz; b) Frequency = 175-180 Hz.

transfer expected from a quasisteady one-dimensional mean and oscillatory flow. The basic approach was to assume that the heat-transfer coefficient is related to the oscillatory mass velocity of the flow,

$$\hat{h}/\bar{h} = \hat{\rho}/\bar{\rho} + \hat{U}/\bar{U} \tag{5}$$

Note that the mean flow velocity for the one-dimensional flow is given by the relation

$$\bar{U}/\bar{a} = (4L/D)\ (Z/L)\bar{M}_w \tag{6}$$

For a cylindrical chamber with acoustically hard walls, the density and velocity oscillations are 90 deg out of phase and are related by the classical acoustic standing wave relations. When these relations, along with Eq. (6), are substituted into

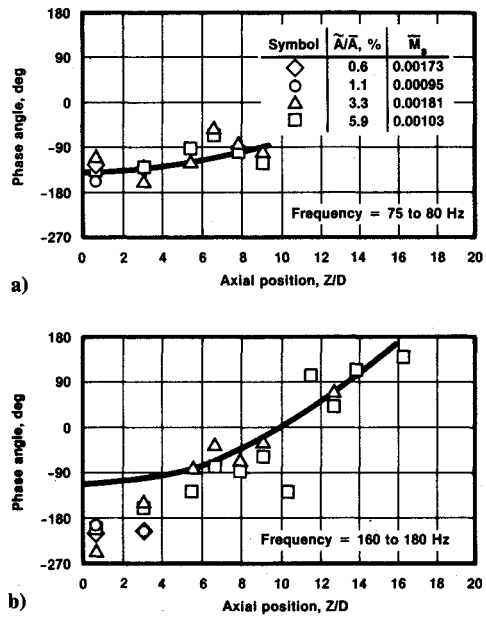

Fig. 20 Phase angle between heat transfer and head-end acoustic pressure: a) Frequency = 75-80 Hz; b) Frequency = 160-180 Hz.

Eq. (5), the resulting equation becomes

$$\left(\frac{\hat{h}}{\bar{h}}\right)=\frac{\hat{P}}{\gamma\bar{P}}\left[\cos\left(\frac{\pi Z}{L}\right)-\frac{i\sin(\pi Z/L)}{4\bar{M}_w Z/D}\right] \tag{7}$$

Parametric studies of Eq. (7) show that the second term on the right-hand side dominates both the magnitude and the phase at the head end. Furthermore, the maximum heat-transfer coefficient is predicted to occur at the head end and to have essentially a constant magnitude over the first third of the axial length. This predicted behavior is consistent with the data suggesting that the acoustic velocity should be normalized to the mean gas speed and not the acoustic speed. From Eq. (7), the oscillatory heat-transfer coefficient would lag the head-end acoustic pressure by 90 deg. However, as shown in Fig. 20, the measured phase angles are -110 to -135 deg. This discrepancy suggests that either the analysis is not correct or that the acoustic waves do not follow the classical forms assumed in the derivation of Eq. (7).

Pulse tests of the chamber showed the acoustic damping of the chamber to be very high (i.e., $\alpha/f>0.3$). This behavior in turn suggests the porous tubing simulating the burning propellant surface produces large acoustic damping. Separate experiments conducted several years ago in a rotating valve confirmed that the admittance of the porous tubing is indeed a large negative number (i.e., -0.02). Hence, the damping from the porous tubing might alter the acoustic wave behavior and account for the phase discrepancy.

To estimate the effect of this admittance on the acoustic velocity and pressure mode shapes, Kummer function solutions for the acoustic wave shape were calculated.[11,35] These solutions permit the effect of the sidewall admittance on the modal behavior to be estimated. The solutions were then substituted into Eq. (5) to estimate the phase angle beween the head-end acoustic pressure and the oscillatory heat-transfer coefficients. The solid lines in Fig. 20 show the predicted phase behavior.

Note that at the lower frequencies, the observed phase behavior follows the predicted behavior with reasonable accuracy. At the higher frequencies, however, substantial deviations are observed, particularly near the head end. This discrepancy suggests additional flow effects are important in this region. Flandro[25,26] and BenReuven[28] have suggested that acoustic boundary-layer effects might also be significant in these flows and might account for the discrepancy between the measured and predicted phase angles.

Finally, it should be emphasized that these studies have addressed only the flowfield aspects of the velocity coupling process. It is interesting to note, however, that magnitudes of the heat-transfer response to the acoustic waves in these cold-flow tests are similar to the magnitude of the heat-transfer responses to the turbulence in the mean flow. Thus, if erosive burning results from turbulence interacting with the combustion zone, as postulated by Beddini, then these cold-flow results should be directly applicable to velocity coupling. It is recognized that no attempt has been made to investigate how these flow processes interact with the propellant combustion zone to produce the burning rate response. This analysis of the combustion effects requires a detailed knowledge of the combustion zone structure, as well as studies on precisely how the acoustic and turbulent fluctuations change the combustion zone. Results from these cold-flow studies do, however, define a realistic starting point for the combustion studies.

Conclusions

The composite results indicate a model for velocity coupling that differs significantly from the models that have been used to interpret motor data and predict stability. The measurements indicate there is a threshold in the mean flow velocity below which acoustic velocity oscillations influence the oscillatory heat-transfer coefficient. Downstream of this threshold, there is no effect of the acoustic velocity on the heat transfer at very low acoustic pressures. This threshold seems to be related to the onset of turbulence, which appears to destroy the effect of the low-amplitude acoustic waves near the wall. Furthermore, nonlinear effects first appear close to the head end of the chamber, not at the location of the threshold velocity.

Based on these results, the model for velocity coupling must be reformulated. This task will require a complete reinterpretation of motor stability predictions. Equally important will be the reassessment of the laboratory burners that have been used to measure velocity-coupled response functions. Finally, the interpretation of nonlinear behavior based on the previous models will need re-evaluation.

Acknowledgment

This work was supported by the U.S. Force Office of Scientific Research under Conract F49620-81-C-0027.

References

[1]Hart, R. W., Bird, J. F., and McClure, F. T., "The Influence of Erosive Burning on Acoustic Instability in Solid Propellant Rocket Motors," *AIAA Progress in Astronautics and Aeronautics: Solid Propellant Rocket Research,* Vol. 1, edited by M. Summerfield, Academic Press, New York, 1960, pp. 423-451.

[2]Price, E. W., "Axial Mode, Intermediate Frequency Combustion Instability in Solid Propellant Rocket Motors," AIAA Paper 64-146, Jan. 1964.

[3]Price, E. W. and Dehority, G. L., "Velocity Coupled Axial Mode Combustion Instability in Solid Propellant Rocket Motors," *Proceedings of ICRPG/AIAA 2nd Solid Propulsion Conference,* AIAA, June 1967, pp. 213-227.

[4]Dehority, G. L. and Price, E. W., "Axial Mode, Intermediate Frequency Combustion Instability in Solid Propellant Rockets," Naval Weapons Center, NWC TP 5654, Oct. 1974.

[5]Culick, F. E. C., "Stability of Longitudinal Oscillations with Pressure and Velocity Coupling in a Solid Propellant Rocket," *Combustion Science and Technology,* Vol. 2, 1970, pp. 179-201.

[6]Lengelle, G., "A Model Describing the Velocity Response of Composite Propellants," *AIAA Journal,* Vol. 13, 1975, pp. 315-322.

[7]Micheli, P. L., "Investigation of Velocity Coupled Combustion Instability," AFPRL-TR-76-100, Jan. 1977.

[8]Condon, J. A., "A Model for the Velocity Coupling Response of Composite Propellants," Paper presented at 16th JANNAF Combustion Conference, Monterey, CA, 1979.

[9]Stepp, E. E., "Effect of Pressure and Velocity Coupling on Low Frequency Instability," *AIAA Journal*, Vol. 5, 1967, pp. 945-948.

[10]Beckstead, M. W. and Butcher, A. G., "The Velocity Coupled T-burner," AIAA Paper 74-200, 1974.

[11]Brown, R. S., Waugh, R. C., and Kelley, V. L., "Rotating Valve for Velocity Coupled Combustion Response Function Measurements," *Journal of Spacecraft and Rockets,* Vol. 19, 1982, pp. 437-444.

[12]Micci, M. M., Caveny, L. H., and Sirignano, W. A., "Linear Analysis of Forced Longitudinal Waves in Rocket Motor Cavities," *AIAA Journal,* Vol. 19, 1981, pp. 198-204.

[13]Crump, J. E. and Price, E. W., "Effects of Acoustic Environment on the Burning Rate of Solid Propellants," *AIAA Journal,* Vol. 2, 1964, pp. 1274-1278.

[14]Nadaud, L. and Gigquel, M., "Effects of Sound Waves on the Burning Rate of Solid Propellants," *La Recherche Aeronautique,* No. 88, 1962, pp. 59-63.

[15]Lovine, R. L., Dudley, D. P., and Waugh, R. C., "Standardized Stability Prediction Method for Solid Rocket Motors," AFPRPL-TR-76-32, 1976.

[16]Glick, R. L. and Kirschner, T. J. Jr., "Combustion Stability of Low L/D Space Motors," AIAA Paper 81-1558, 1981.

[17]Brown, R. S., Waugh, R. C., and Willoughby, P. G., "IUS Combustion Instability Studies," CPIA Pub. 329, Vol. 3, 1980, pp. 297-325.

[18]Price, E. W., "Velocity Coupling in Oscillatory Combustion of Solid Propellants," *AIAA Journal,* Vol. 17, 1979, pp. 799-800.

[19]Culick, F. E. C., "Rotational Axisymmetric Mean Flow and Damping of Acoustic Waves in Solid Propellant Motors," *AIAA Journal,* Vol. 4, 1966, pp. 1462-1464.

[20]Beddini, R. A., "Analysis of Injection—Induced Flows in Porous Walled Ducts with Application to the Aerothermochemistry of Erosive Burning," Ph.D. Thesis, Rutgers University, New Brunswick, NJ, Oct. 1981.

[21]Dunlap, R., Willoughby, P. G., and Hermsen, R. W., "Flow Field in the Combustion Chamber of a Solid Propellant Rocket Motor," *AIAA Journal,* Vol. 12, 1974, pp. 1440-1442.

[22]Gostintsev, Y. A. and Pokhil, P. F., "Relation of Two Combustion Anomolies of Porous Tubes," *Doklady Akademii Nauk SSR,* Vol. 188, No. 1, 1969, pp. 135-136.

[23]Medvedev, Y. I. and Revyagin, L. N., "Unsteady Erosion of a Powder," *Fizika Goreniya i Vzryva,* Vol. 10, No. 3, 1974, pp. 341-345.

[24]Beckstead, M. W., "Workshop Report: Velocity Coupling," CPIA Pub. 329, Vol. 1, 1980, pp. 195-200.

[25]Flandro, G. A., "Solid Propellant Acoustic Admittance Correlations," *Journal of Vibration and Sound,* Vol. 36, 1974, pp. 297-312.

[26]Flandro, G. A., "Nonlinear Time-Dependent Combustion of a Solid Propellant Rocket," CPIA Pub. 366, Vol. 2, 1982, pp. 111-122.

[27]Hegde, U. G., Chen, F. L., and Zinn, B. T., "Investigation of Reactive and Non-Reactive Acoustic Boundary Layers in Porous Walled Ducts," CPIA Pub. 412, Vol. 1, 1984, pp. 91-102.

[28]BenReuven, M., "The Viscous Wall-Layer Effect in Injected Porous Pipe Flow," *AIAA Journal,* Vol. 24, 1986, pp. 284-292.

[29]Dunlap, R., Willoughby, P. G., and Young, S. W., "Cold Flow Studies Test Report," United Technologies Corp., Chemical Systems Div. San Jose, CA, Rept. CSD 4901-79-135, 1980.

[30]Brown, R. S., Dunlap, R., Young, S. W., and Waugh, R. C., "Vortex Shedding as a Source of Acoustic Energy in Segmented Solid Rockets," *Journal of Spacecraft and Rockets,* Vol. 18, pp. 312-319.

[31]Brown, R. S., Erickson, J. E., and Babcock, W. R., "Combustion Response Function Measurements by the Rotating Valve Method," *AIAA Journal,* Vol. 12, 1974, pp. 1502-1510.

[32]Taylor, G., "Fluid Flow in Regions Bounded by Porous Surfaces," *Proceedings of the Royal Society, London,* Vol. 234A, 1956, pp. 456-475.

[33]Yagodkin, V. L., "Use of Channels with Porous Walls for Studying Flows Which Occur During Combustion of Solid Propellants," *Proceedings of the 18th Astronautics Conference,* USSR, Vol. 3, 1967, pp. 69-79.

[34]Dunlap, R. et al., "Internal Flow Field Investigation," CPIA Pub. 420, Vol. 2. 1984, pp. 200-201.

[35]Brown, R. S., "Coupling Between Velocity Oscillations and Solid Propellant Combustion," United Technologies Corp., Chemical Systems Div., San Jose, CA, Rept. 2749-AR-3, Aug. 1984.